Calculation Method of Thermal Neutron Scattering Law Data for Liquid Materials in NECP-Atlas

Yutu Ma, Tiejun Zu*, Chengyao Wu, Liangzhi Cao, Hongchun Wu
School of Nuclear Science and Technology, Xi'an Jiaotong University, Xi'an, Shaanxi 710049, China
**Corresponding author: tiejun@mail.xjtu.edu.cn*

Keywords : thermal neutron scattering law, molecular dynamics, liquid materials, atomic trajectory, NECP-Atlas

1. Introduction

The calculation of the thermal neutron scattering law data (TSL) of liquid materials is complicated because of the complex motion behavior of atoms. In addition to the collective vibration of atoms, there are also diffusion motion and intramolecular rotation/stretching motion. Traditional method based on incoherent approximation and Gaussian approximation decomposes the rigorous TSL computational model into phenomenological models such as phonon expansion model, diffusion model and rotation/stretch model, which have inherent approximations.

To eliminate the shortcomings of traditional methods, such as splitting the motion modes and selecting the diffusion model according to the user's experience, a method for directly calculating TSL of liquid materials based on atomic trajectories is established by using the atomic trajectories calculated by classical molecular dynamics (MD) simulation. The new method was applied to nuclear data processing code NECP-Atlas [1] and verified based on the calculation of TSL data of H_2O and D_2O.

2. The theory of calculation method

In this section the theory of the calculation method of TSL data based on atomic trajectories is described. Since quantum effects are not considered in the atomic trajectories obtained from the MD simulation of classical mechanics, the relation between the thermal scattering law of classical mechanics and quantum mechanics is established by constructing the characteristic function, and then the scattering law data considering quantum effects is obtained by quantum correction based on the atomic trajectories calculated by classical mechanics.

2.1 The Double Differential Cross Section

The double differential cross section is defined as:

$$(1)\ \sigma(E \to E', \mu) = \frac{\sigma_{\mathrm{b}}}{2k_{\mathrm{B}}T}\sqrt{\frac{E'}{E}}S_{\mathrm{tot}}(\alpha,\beta)$$

where E is the incident energy, E' is the outgoing energy, k_B is the Boltzmann constant, T is the temperature, μ represents the cosine of scattering angle in the laboratory frame, and $S_{\mathrm{tot}}(\alpha,\beta)$ is the total thermal scattering law, which is composed of the self-scattering law $S_s^q(\alpha,\beta)$ and the distinct thermal scattering law $S_d^q(\alpha,\beta)$:

$$(2)\ S_{\mathrm{tot}}(\alpha,\beta) = \frac{\sigma_{\mathrm{coh}}}{\sigma_{\mathrm{b}}}S_d^q(\alpha,\beta) + S_s^q(\alpha,\beta)$$

Here, q denotes the quantum mechanics, σ_{coh} is the coherent bound atom scattering cross section, and σ_{b} is the bound atom scattering cross section.

2.2 The Quantum-Corrected Self-Scattering Law

The quantum-corrected self-scattering law $S_s^q(\alpha,\beta)$ is formulated by:

$$(3)\ S_s^q(\alpha,\beta) = \frac{1}{2\pi}\int_{-\infty}^{\infty} I_s^q(\alpha,t')\exp(-i\beta t')dt'$$

where α and β are the unitless momentum and energy transfer variables, respectively; $I_s^q(\alpha,t')$ is the intermediate scattering function of quantum mechanics, which is defined by:

$$(4)\ I_s^q(\alpha,t') = e^{-\alpha\gamma(t')}$$

and t' is given by:

$$(5)\ t' = t/(\hbar/k_{\mathrm{B}}T)$$

where $\hbar$ is the Planck constant.

With the Fourier transform of $f^q(\beta)$, the width function $\gamma(t')$ in Eq. (4) is obtained:

$$(6)\ \gamma(t') = \int_{-\infty}^{\infty} e^{-i\beta t'} f^q(\beta)d\beta$$

According to the relation between the characteristic function of classical mechanics and quantum mechanics, the characteristic function of quantum mechanics $f^q(\beta)$ is obtained based on the characteristic function of classical mechanics $f^c(\beta)$:

$$(7)\ f^q(\beta) = \frac{\beta e^{\beta/2}}{2\sinh(\beta/2)}\cdot f^c(\beta) + i\frac{\beta}{2}\cdot f^c(\beta)$$

With the mean squared displacement (MSD) $\delta r^2(t)$ calculated based on the atomic trajectories obtained from the MD simulation, the characteristic function of classical mechanics $f^c(\beta)$ is calculated by:

$$(8)\ f^c(\beta) = \frac{Mk_{\mathrm{B}}T}{3\hbar^2}\int_{-\infty}^{\infty} e^{i\beta t'}\delta r^2(t')dt'$$

Therefore, the-scattering law of quantum mechanics can be obtained based on the MSD calculated based on atomic trajectories calculated by classical mechanics.

2.3 The Distinct Thermal Scattering Law

ZHU [2] considers the distinct thermal scattering law by constructing the collective structure factors, while this paper proposes a more convenient calculation method based on the atomic trajectories obtained from the MD simulation.

The distinct thermal scattering law is calculated as follows:

$$(9)\ S_d^q(\alpha,\beta) = S_s^q(\alpha/\tilde{S}_i(\kappa),\beta)\tilde{S}_i(\kappa) - S_s^q(\alpha,\beta)$$

Radial distribution function (RDF) obtained by atomic trajectories is used to calculate the dynamic structure factor for each type of atom.

$$(10)\ \tilde{S}_i(\kappa) - 1 = \frac{\sum_j c_j b_{\mathrm{coh}}^i b_{\mathrm{coh}}^j \left[S_{ij}(\kappa) - 1\right]}{\left(b_{\mathrm{coh}}^i\right)^2}$$

where $\tilde{S}_i(\kappa)$ is the partial dynamic structure factor of the *i*-th atom, c_j is the mole fraction of *j*-th atom, b_{coh}^i and b_{coh}^j denote the coherent bound scattering length of the *i*-th atom and *j*-th atom respectively.

The partial dynamic structure factor $S_{ij}(\kappa)$ between the *i*-th atom and *j*-th atom is obtained based on RDF between the *i*-th atom and *j*-th atom $g_{ij}(r)$:

$$(11)\ S_{ij}(\kappa) = 1 + 4\pi\rho\int_0^\infty dr\left[g_{ij}(r) - 1\right]r^2\frac{\sin(\kappa r)}{\kappa r}$$

where ρ is the density of atoms in the simulated system, r is the distance between atoms and κ is the wave vector transfer variable.

According to the equations shown above, the relation between RDF obtained by atomic trajectories and the double differential cross section is established, and the distinct thermal scattering law can be obtained based on the RDF calculated based on the atomic trajectories obtained from the MD simulation.

3. Numerical verification

Taking H_2O and D_2O as examples, the calculation method of TSL data based on atomic trajectory was numerically verified with microscopic cross sections and macroscopic benchmarks in this section.

3.1 Molecular Dynamics Simulation

GROMACS [3], a software suite for MD and output analysis, was used to obtain the atomic trajectories of H_2O and D_2O. In the periodical boundary condition, the TIP4P/2005f model of H_2O was used to conduct MD simulation with 515 molecules filled into a 2.5mm×2.5mm×2.5mm box.

The MD simulation can be divided into four steps: the energy minimization, the equilibration of canonical ensemble (NVT), the equilibration of constant-pressure and constant-temperature ensemble (NPT), and the final run which writes the atomic trajectories to a file. The method of Velet was selected to generate a pair list with buffering and the method of Particle-Mesh Ewald (PME) was selected in coulombtype. The cut-off radius of Leonard Jones and Van der Waals was set to 0.9 nm. The NVT ensemble at 293.6K and NPT ensemble at 293.6K and 1 bar was selected. Temperature coupling selected was a Nose-Hoover extended ensemble and pressure coupling selected was Parrinello-Rahman pressure coupler. The time constants for temperature coupling and pressure coupling were 0.1ps and 0.5ps. The compressibility was 4.5e-5bar-1. The MD simulation of D_2O is similar to H_2O except for the changed mass of H.

3.2 Simulation Outputs

The main input parameter of the calculation method based on atomic trajectories is MSD, which can be obtained from the trajectory of atom. Fig. 1 and Fig. 2 shows the MSD of H in H_2O and D in D_2O obtained from the simulations of 0.1ps and 10ps, respectively. Atoms of H are not subject to the action of adjacent atoms in the time region from 0 to 0.03ps, showing free gas diffusion behavior. While H gradually interact with adjacent atoms from 0.03 to 0.06ps, and the free gas diffusion behavior is hindered. After 0.06ps, the curve becomes linear. Fig. 2 shows that D in D_2O also has the same diffusion behavior.

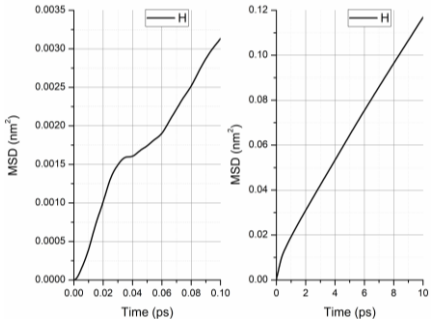

Fig. 1 The MSD of H in H_2O at 293.6K

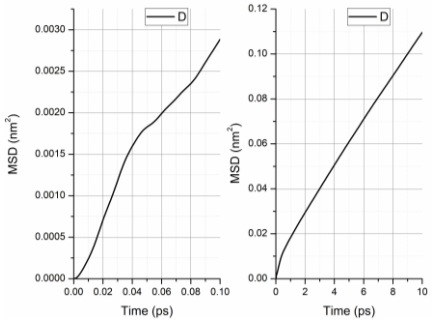

Fig. 2 The MSD of D in D_2O at 293.6K

The distinct thermal scattering law for D_2O should be considered, as σ_{coh} occupies a considerable proportion of σ_b for D_2O. Calculated RDF and partial dynamic structure factor of D_2O are presented in Fig. 3 and Fig. 4 respectively.

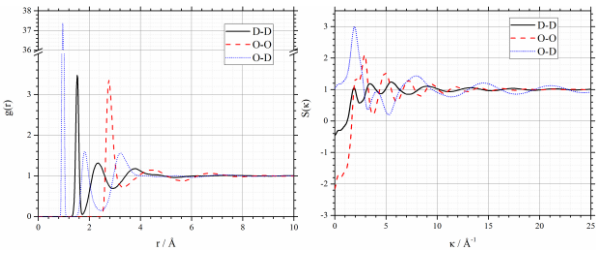

Fig. 3 RDF and partial structure factor for D_2O at 293.6K

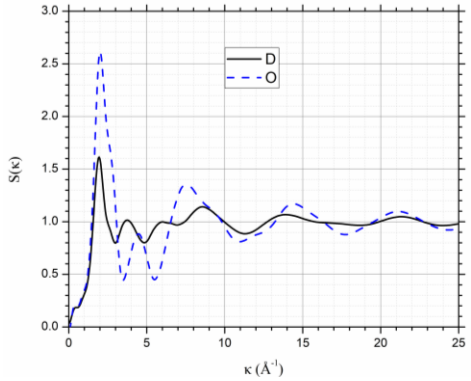

Fig. 4 Partial structure factor for D and O of D_2O at 293.6K

3.3 Thermal Scattering Cross Section

The double differential cross sections of H_2O for 4 groups of incident energy and scattering angle were calculated with the method based on atomic trajectories and presented in Fig. 5 in comparison to TSL data in evaluated nuclear data files (ENDF) [4] and results in The Experimental Nuclear Reaction Data (EXFOR) [5].

As can be seen, the double differential cross sections calculated based on atomic trajectories exhibit good agreement with ENDF/B-VIII.0. Fig. 5 (b) shows that the results with the method based on atomic trajectories agree well with ENDF/B-VIII.0 and deviate slightly more from the EXFOR data. As shown in the other partial graphs of Fig. 5, results of this work and ENDF/B-VIII.0 show better results in comparison with the data from ENDF/B-VII.1.

Fig. 6 shows the double differential cross sections of D_2O obtained by this work in comparison to the experimental data from EXFOR. The results calculated based on atomic trajectories shows good agreement with data of ENDF/B-VIII.0 and are closer to experimental results compared to ENDF/B-VII.1.

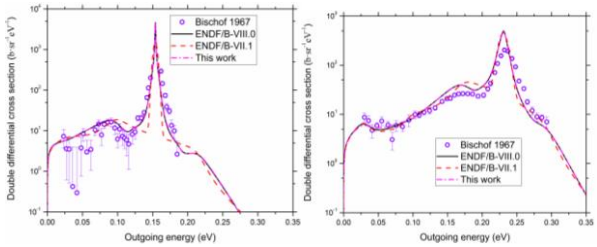

(a) E=0.154eV θ=14° (b) E=0.231eV θ=25°

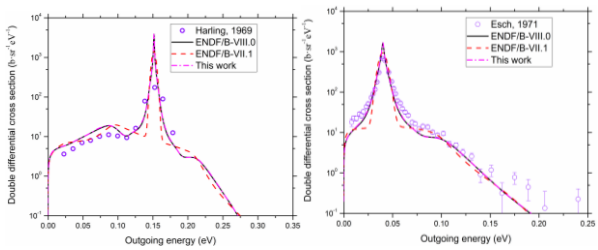

(c) E=0.1515eV θ=15° (d) E=0.04eV θ=40°

Fig. 5 Double differential cross section of H_2O at 293.6K

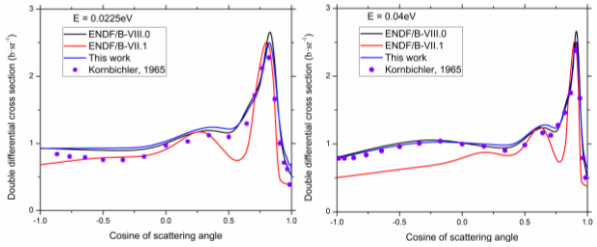

(a) E=0.0225eV (b) E=0.04eV

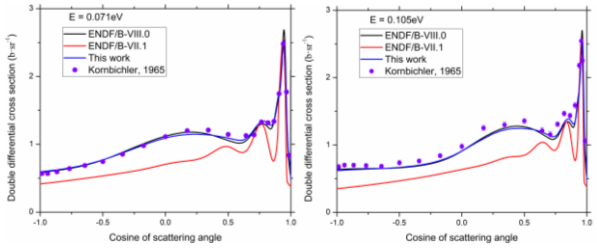

(c) E=0.071eV (d) E=0.105eV

Fig. 6 Double differential cross section of D_2O at 293.6K

Fig. 7 and Fig. 8 show the total cross section of H_2O and D_2O, respectively. As demonstrated by Fig. 7, the total cross sections calculated based on atomic trajectories and data from ENDF/B-VIII.0 agree well with the experimental data, while the total cross section calculated based on ENDF/B-VII.1 deviates from the experimental data in the 10^{-5}-10^{-3}ev energy region. As presented in Fig. 8, the total cross section of D_2O shows a peak near the incident energy of 0.003ev. The total cross sections of D_2O calculated based on atomic trajectories and data from ENDF/B-VIII.0 are closer to the experimental data from EXFOR in the energy

region of 0.0004-0.002ev compared with the data of ENDF/B-VII.1.

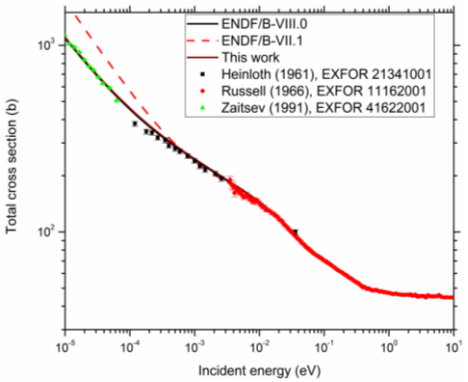

Fig. 7 The total cross section of H_2O at 293.6K

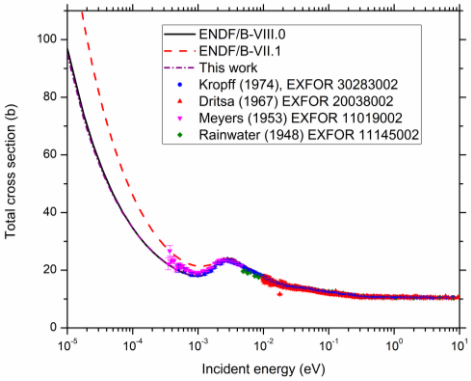

Fig. 8 The total cross section of D_2O at 293.6K

3.4 Calculations of ICSBEP Benchmarks

To evaluate the effect of TSL data for H_2O and D_2O calculated using different methods on neutronics calculation, 48 and 56 benchmarks respectively using H_2O and D_2O as moderator or reflector from International Criticality Safety Benchmark Evaluation Project (ICSBEP) [6] were analyzed. Monte Carlo code NECP-MCX [7] is adopted to perform neutronics calculations. The absolute value of statistical uncertainties of k_{eff} was controlled within 20pcm, and all data from ENDF/B-VIII.0 was used in neutronics calculation except for the thermal scattering cross section data of H_2O and D_2O.

Fig. 9 and Fig. 11 show the ratio of calculation values and experiment values (C/E) of the multiplication factor k_{eff} for ICSBEP benchmarks, which are calculated as:

(12) $C/E = k_{\text{eff}}^{\text{calc}} / k_{\text{eff}}^{\text{bench}}$

The C/E values of k_{eff} for ICSBEP benchmarks of H_2O are shown in Fig. 9. Overall, the results of k_{eff} calculated with the TSL data obtained from the atomic trajectories agree well with the results using TSL data from ENDF/B-VIII.0 and show improvement compared to the results of ENDF/B-VII.1.

Fig. 10 shows the deviation of k_{eff} for ICSBEP benchmarks of H_2O calculated by using TSL data from ENDF files compared with calculation method based on atomic trajectories. The maximum of the absolute value of deviation of k_{eff} for ICSBEP benchmarks from results of ENDF/B-VIII.0 is 68pcm, happening in IST001_02 and PST002_04 benchmarks, and the results of deviation of 35 benchmarks are less than two times the standard deviation of Monte Carlo calculation. For the results of ENDF/B-VII.1, absolute value of maximal deviations is 263pcm, happening in HMT006_08, and the deviations of 11 benchmarks are larger than 100pcm.

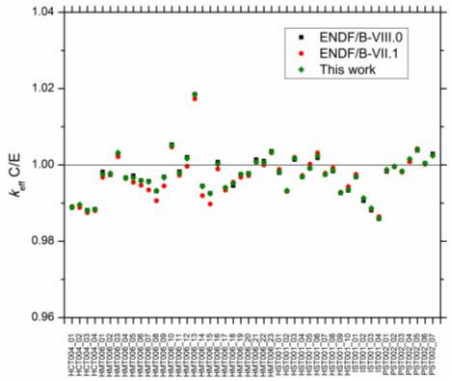

Fig. 9 C/E of k_{eff} for ICSBEP benchmarks containing H_2O

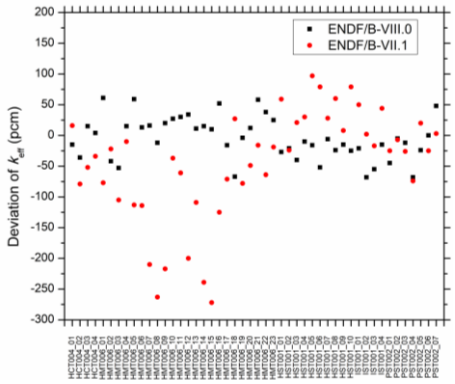

Fig. 10 Deviation of k_{eff} of ICSBEP benchmarks of H_2O compared with atomic trajectories based method

Fig. 11 shows the C/E values of k_{eff} for ICSBEP benchmarks of D_2O. The results calculated with the TSL data obtained from atomic trajectories are in good agreement with the results calculated with ENDF/B-VIII.0 data, and the values of C/E obtained by this work is closer to 1 compared with results calculated with TSL data for D_2O from ENDF/B-VII.1.

The deviations of k_{eff} for ICSBEP benchmarks of D_2O calculated by using TSL data from ENDF files compared with calculation method based on atomic trajectories are shown in Fig. 12. The absolute value of maximal deviation from results of ENDF/B-VIII.0 is 90pcm, happening in LMT015_22 benchmark, and the deviations of 39 benchmarks are less than two times the standard deviation. For ENDF/B-VII.1, the absolute value of maximal deviation compared with this work is

884pcm, happening in HCT017_01 benchmark. The deviations of 53 benchmarks are larger than 100pcm.

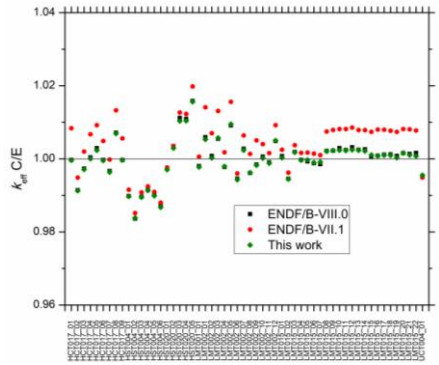

Fig. 11 C/E of k_{eff} for ICSBEP benchmarks containing D_2O

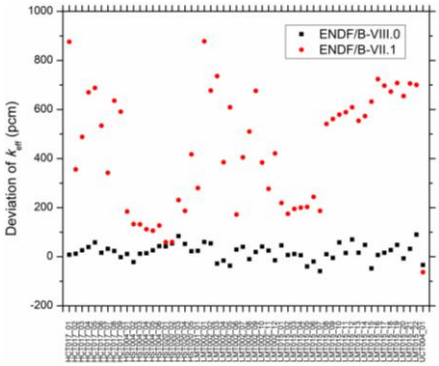

Fig. 12 Deviation of k_{eff} of ICSBEP benchmarks of D_2O compared with atomic trajectories based method

The root mean squared errors (RMSE) of the results for ICSBEP benchmarks are presented in Table 1. The smaller the RMSE represents the closer to the experimental values. For H_2O and D_2O, the results of RMSE all show that the data obtained by this work has slight improvement compared with ENDF/B-VIII.0 and demonstrate a considerable improvement compared to ENDF/B-VII.1.

Table I: Root Mean Squared Errors

	This work	ENDF/B-VIII.0	ENDF/B-VII.1
H_2O	619.5531	628.3943	647.8772
D_2O	629.1274	637.4075	866.1761

4. Conclusions

The calculation method of TSL data for liquid materials based on atomic trajectories is established in nuclear data processing code NECP-Atlas. The developed calculation method based on the atomic trajectories is verified based on the TSL data of H_2O and D_2O in ENDF/B-VIII.0 and the experimental data from EXFOR. According to the RMSE of k_{eff} calculated, the accuracy of the thermal scattering cross sections obtained from atomic trajectories shows slight improvement compared with ENDF/B-VIII.0, exhibiting good agreement with the experimental data. Comparing with ENDF/B-VII.1, the results of ICSBEP benchmarks with the calculation method based on atomic trajectories demonstrate a visible improvement of k_{eff}.

ACKNOWLEDGEMENTS

This research is supported by National Natural Science Foundation of China (No. 12075183 & 12135019), National Key R&D Program of China (No. 2022YFB1902600)

REFERENCES

[1] Tiejun Zu, Jialong Xu, Yongqiang Tang, et al, NECP-Atlas: A new nuclear data processing code, Annals of Nuclear Energy, Vol. 123, pp 153-161, 2019.
[2] ZHU Y, Analysis of Neutron Thermalization in Liquid FLiBe, North Carolina State University, 2018.
[3] Van Der Spoel D, Lindahl E, Hess B, et al, GROMACS: Fast, Flexible, and free, Journal of Computational Chemistry, Vol. 26, pp 1701-1718, 2005.
[4] Brown D, Chadwick M, Capote R, et al, ENDF/B-VIII.0: The 8th major release of the nuclear reaction data library with CIELO-project cross sections, new standards and thermal scattering data, Nuclear Data Sheets, Vol. 148, pp 1-142, 2018.
[5] Otuka N, Dupont E, Semkova V, et al, Toward more complete and accurate experimental nuclear reaction data library (EXFOR): International collaboration between nuclear reaction data centres (NRDC), Nuclear Data Sheets, Vol. 120, pp 272-276, 2020.
[6] Briggs, J.B, Dean, V.F and Scott, L, The International Criticality Safety Benchmark Evaluation Project, Proceedings of The Fifth International Conference on Nuclear Criticality Safety, Sept. 17-21, 1995, Albuquerque, NM.
[7] Qingming He, Qi Zheng, Jie Li, et al, NECP-MCX: A hybrid Monte-Carlo-Deterministic particle-transport code for the simulation of deep-penetration problems, Annals of Nuclear Energy, Vol. 151, 2021.